THE JOURNAL OF PHYSICAL CHEMISTRY LETTERS
A JOURNAL OF THE AMERICAN CHEMICAL SOCIETY

pubs.acs.org/JPCL
Letter

Processing and Functionalization of Vertical Graphene Nanowalls by Laser Irradiation

Stefanos Chaitoglou,* Argyro Klini, Nikandra Papakosta, Yang Ma, Roger Amade, Panagiotis Loukakos, and Enric Bertran-Serra

Cite This: J. Phys. Chem. Lett. 2024, 15, 3779−3784
Read Online

ACCESS | Metrics & More | Article Recommendations | Supporting Information

ABSTRACT: The processing of vertical graphene nanowalls (VGNWs) via laser irradiation is proposed as a means to modulate their physicochemical properties. The effects of the number of applied pulses and fluence of each pulse are examined. Raman spectroscopy studies the effect of irradiation on the chemical structure of the VGNWs. Results show a decrease in density of defects and number of layers, which points toward a mechanism including evaporation of amorphous or loosely bonded C from defective points and recrystallization of graphene. Moreover, the effect of laser irradiation parameters on the morphology of Mo thin films deposited on VGNWs is investigated. The received thermal dosage results in the formation of particles. In this case, the number of pulses and pulse fluence are found to affect the size and distribution of these particles. The study provides a novel approach for the functionalization of VGNWs via laser irradiation, which can be extended to other graphene-based nanostructures.

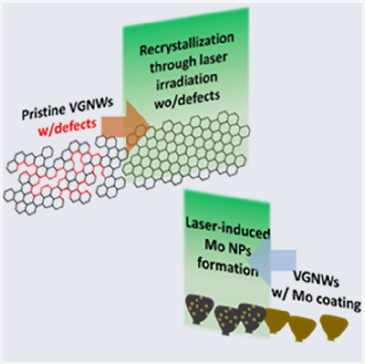

Graphene and graphene-related materials have been extensively studied during the course of the last 15 years, and nowadays, we possess a good understanding of their rich physical and chemical properties.[1] Therefore, these materials have been used in a vast range of applications, like in nanoelectronics, energy harvesting and storage, and sensors, and as composite materials.[2−4] Modulation of the intrinsic properties of the graphene nanostructures can be beneficial to match the requirements of specific applications.[5,6] For graphene prepared through vapor deposition techniques, like chemical vapor deposition,[7] *in situ* modulation of these properties during the growth is challenging, thus post-growth processing is often preferred. In the above context, processing via laser irradiation has emerged as a versatile, non-contact, programmed processing method, which offers precise physical and chemical property regulation.[8] Examples of applications are the use of a laser for the reduction of graphene oxide,[9] the modulation of defect density present on the graphene lattice,[10] and the preparation of so-called laser-induced graphene (LIG), which occurs via irradiation of a polyimide film by a CO_2 laser and has been extensively used for the preparation of three-dimensional graphene electrodes for supercapacitors.[11−13]

Vertical graphene nanowalls (VGNWs), also known as carbon nanowalls,[14] are a three-dimensional graphene derivative, in which few-layer graphene sheets are deposited perpendicularly to the growth substrate. They possess a very large surface area and high conductivity, which makes them attractive as electrochemical electrodes[15,16] and gas sensors.[17] VGNWs are typically synthesized using plasma-enhanced chemical vapor deposition (PECVD) technology, mainly by microwave (MW), radio-frequency (RF) plasma, and inductively coupled plasma (ICP).[18] Functionalization of the VGNWs occurs by decorating them with transition metal carbide and oxide particles for the preparation of hybrid structures that are very efficient in electrocatalysis, batteries, and supercapacitor applications.[19−22] Taking into consideration the vast reach of applications, tuning of the physicochemical properties of VGNWs may be required. Modulation and functionalization via laser processing can be a fast and non-destructive method that is fitted in the above purpose. As proof of principle, here, we present results on the post-growth laser irradiation of pristine VGNWs in an inert atmosphere and its effect on the Raman fingerprint of the VGNWs. In addition, we investigate the effect of laser irradiation on molybdenum (Mo) thin films previously deposited on the VGNWs and the subsequent formation of particles as a result of Mo dewetting and clustering.

The setup of the laser irradiation experiments is illustrated in Figure 1a. A detailed description of the material preparation, conditions of laser irradiation experiments with pulses with the duration of few nanoseconds, and physicochemical characterization is included in the Supporting Information and previous works.[23,24] Scanning electron microscopy (SEM) character-

Received: January 19, 2024
Revised: February 21, 2024
Accepted: March 5, 2024
Published: March 29, 2024

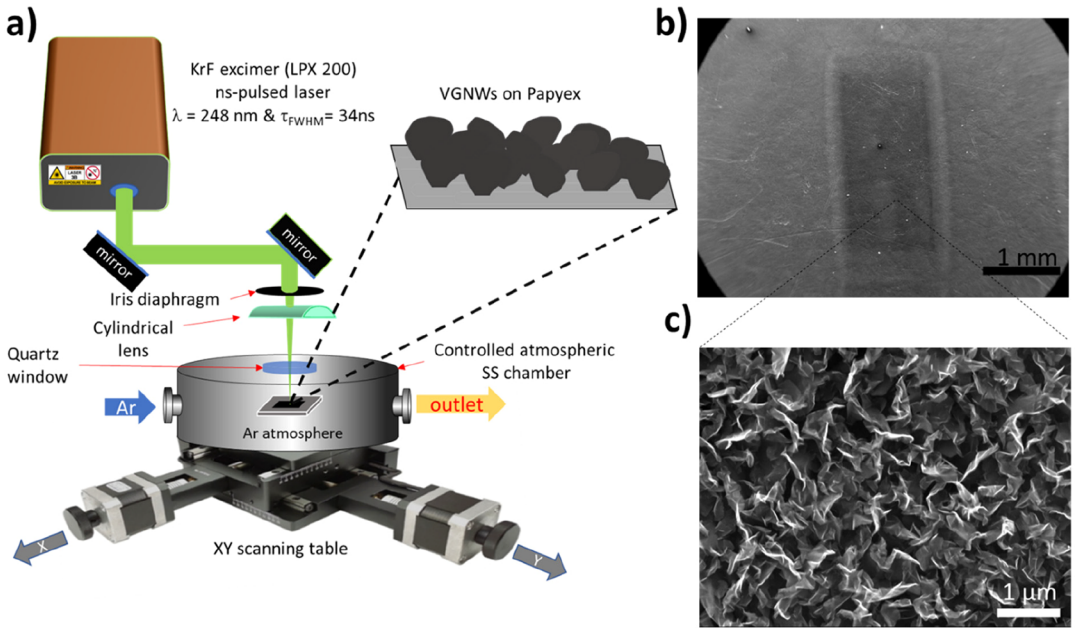

Figure 1. (a) Schematic illustration of the experimental setup used for the laser irradiation of the VGNW samples. (b) SEM image of the irradiated area of the sample. The scale bar is 1 mm. (c) SEM image with a top view of the VGNWs upon irradiation (100 pulses of 0.186 J cm^{-2} fluence). The scale bar is 1 μm.

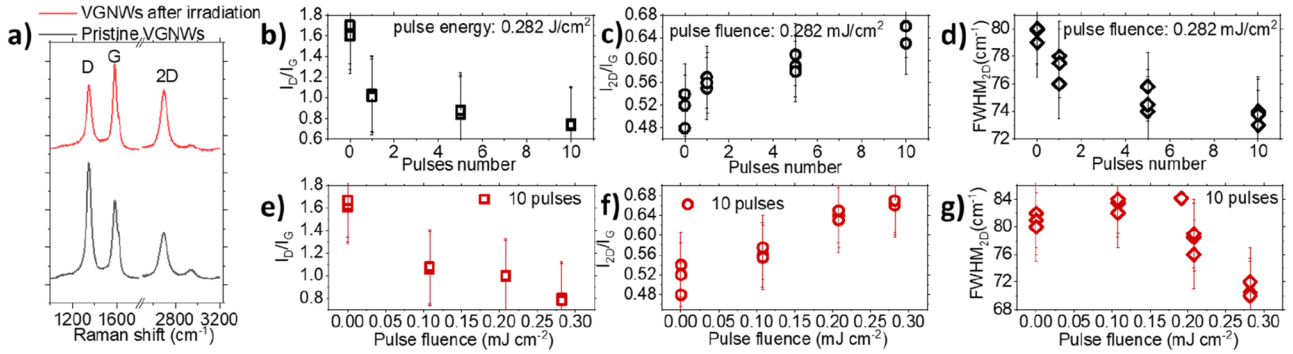

Figure 2. Raman spectroscopy characterization of the pristine and irradiated samples. (a) Raman spectra of pristine VGNWs (black spectrum) and upon irradiation (red spectrum). (b) Evolution of I_D/I_G, (c) I_{2D}/I_G, and (d) $fwhm_{2D}$ with respect to the number of pulses for a fixed pulse fluence value. (e) Evolution of I_D/I_G, (f) I_{2D}/I_G, and (g) $fwhm_{2D}$ with respect to the fluence of pulses for a fixed number of 10 applied pulses.

ization of the substrate reveals a contrast between irradiated and non-irradiated areas (Figure 1b). Nevertheless, a magnified image shows no ablation or structural degradation of the VGNWs present in the irradiated area (Figure 1c). A SEM image of pristine VGNWs is exhibited for comparison in Supplementary Figure 1 of the Supporting Information. Thus, the observed contrast is anticipated to be due to variation in charge carrier doping related to VGNW surface chemistry.[25]

Upon irradiation, samples were characterized by Raman spectroscopy to evaluate the modification in the crystal quality of the graphene lattice. The studied parameters were the laser pulse fluence per sample area and the number of applied pulses. Raman spectra of pristine VGNWs (black graph) and VGNWs upon irradiation (red graph) are exhibited in Figure 2a. Three main peaks associated with graphene are distinguishable. The D band, centered at ~1347 cm^{-1}, is related to the presence of structural defects, vacancies, and boundaries that are present in the graphene crystal and activate the breathing mode of hexagonal carbon rings. On the other hand, the G band, centered at 1580 cm^{-1}, corresponds to the doubly degenerate E_{2g} phonon at the Brillouin zone center. The 2D band is centered at ~2696 cm^{-1} and arises as the second order of the D band. It is manifested in a single peak in monolayer graphene, whereas it splits in four bands in bilayer graphene.[26] A comparison of the spectra in Figure 2a makes a decrease in the D band intensity of the irradiated sample evident with respect to the intensity of the D band in the pristine sample. This indicates a decrease in structural defect density upon irradiation, because this can be calculated taking into consideration the intensity ratio between the D and G modes, I_D/I_G. Briefly, the density of defects can be calculated by the following equation:

$$n_D\ (\mathrm{cm}^{-2}) = \frac{(1.8 \pm 0.5) \times 10^{22} \times \left(\frac{I_D}{I_G}\right)}{\lambda_L^{\ 4}} \quad (1)$$

where λ is the laser wavelength in nanometers.[27,28] It is assumed that evaporation of loosely bonded species on defective graphene sites occurs during laser irradiation. This is followed by a recrystallization process, which explains the

https://doi.org/10.1021/acs.jpclett.4c00193
J. Phys. Chem. Lett. 2024, 15, 3779−3784

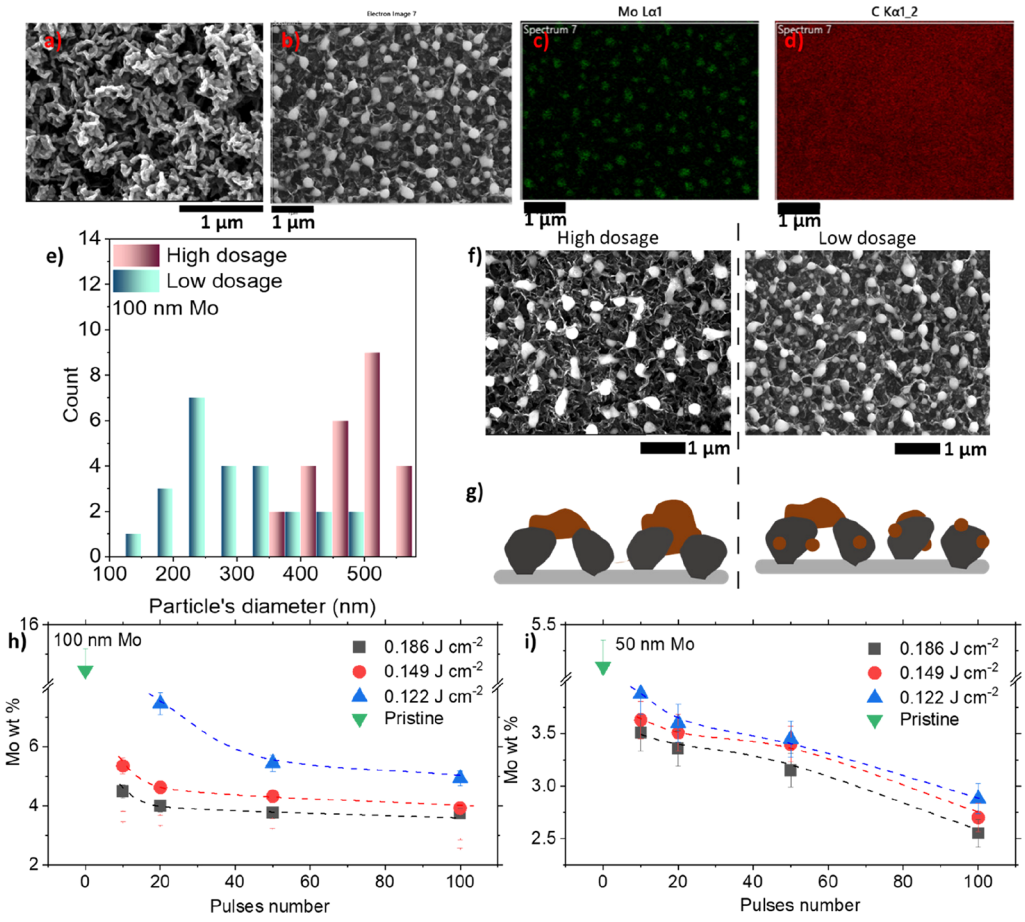

Figure 3. (a and b) SEM images of a 50 nm thick Mo film deposited on VGNWs in (a) pristine state and (b) upon irradiation. (c and d) EDS elemental mapping of C and Mo distributed on the irradiated sample. (e) Size distribution histogram of the formed Mo particles formed in two distinguished irradiation conditions. (f and g) SEM images and schematic representations of the samples resulting from the above distinguished irradiation conditions. (h and i) Mo weight percentage calculated by EDS for pristine samples with (h) 100 nm and (i) 50 nm thick Mo films, as a function of the number and fluence of applied laser pulses.

decrease in the density of defects present in the graphene lattice.[29] The characteristics in terms of intensities and widths of these peaks provide insight regarding the crystal quality of the graphene nanosheets. Here, Raman spectra are analyzed to extract the following information: (i) the thickness of the VGNW flakes, estimated by the full width at half maximum of the graphene 2D peak ($fwhm_{2D}$) and I_{2D}/I_G,[30] and (ii) the density of defects, estimated by I_G/I_D.[27] Results are presented in panels b–g of Figure 2. Three spectra are recorded for each experimental condition. Panels b–d of Figure 2 show the evolution of I_D/I_G, I_{2D}/I_G, and $fwhm_{2D}$ with respect to the number of pulses for a fixed pulse fluence of 0.282 J cm^{-2} as well as the data for the pristine VGNW sample. The observed trend confirms the mechanism that has been described above. Specifically, I_D/I_G decreases from ∼1.6 for the pristine sample to ∼0.7 for the samples irradiated with 10 pulses with a maximum fluence of 0.282 J cm^{-2} (Figure 2b). This trend indicates a decrease in defect density, according to eq 1. I_{2D}/I_G increases from ∼0.52 for the pristine sample to ∼0.66 for the samples irradiated with 10 pulses with a maximum fluence of 0.282 J cm^{-2} (Figure 2c). The $fwhm_{2D}$ decreases from ∼80 cm^{-1} for the pristine sample to ∼73 cm^{-1} for the samples irradiated with 10 pulses with a maximum fluence of 0.282 J cm^{-2} (Figure 2d). These trends indicate a decrease in the number of graphene layers that form the VGNW flakes. Panels e and f of Figure 2 show the evolution of I_D/I_G, I_{2D}/I_G, and $fwhm_{2D}$ with respect to pulse fluence. All samples were irradiated with 10 pulses. The data of pristine VGNW samples are included in the graphs. The observed trend confirms the mechanism that has been described above. Specifically, I_D/I_G decreases from ∼1.65 for the pristine sample to ∼0.81 for the samples irradiated with 10 pulses with a maximum fluence of 0.282 J cm^{-2} (Figure 2e). This trend indicates a decrease in defect density, according to eq 1. I_{2D}/I_G increases from ∼0.52 for the pristine sample to ∼0.67 for the samples irradiated with 10 pulses with a maximum fluence of 0.282 J cm^{-2} (Figure 2f). The $fwhm_{2D}$ decreases from ∼80 cm^{-1} for the pristine sample to ∼69 cm^{-1} for the samples irradiated with 10 pulses with a maximum fluence of 0.282 J cm^{-2} (Figure 2g). Spectra from samples irradiated with pulses of lower energy provide an intermediate to the above values. Conclusively, with the control of the laser fluence and number of applied pulses, the crystal quality of the VGNWs can be modified on demand. This feature can serve for the tuning of the physicochemical properties of the VGNWs and has important implications on their use on energy storage, catalysis, and sensing applications.[31]

Mo thin films with thicknesses of 50 and 100 nm were deposited on the VGNWs via magnetron sputtering. A SEM image of the pristine Mo (50 nm)/VGNW compound is

https://doi.org/10.1021/acs.jpclett.4c00193
J. Phys. Chem. Lett. 2024, 15, 3779−3784

shown in Figure 3a. Samples were irradiated by a laser source, with varying numbers of pulses and laser fluence. During irradiation, dewetting and ripening of the Mo thin film occurs[32] and results in the formation of Mo particles with a very narrow size distribution. A SEM image of an irradiated Mo (50 nm)/VGNW compound is shown in Figure 3b. Panels c and d of Figure 3 show energy-dispersive X-ray spectroscopy (EDS) mapping images of Mo and C, confirming the formation of Mo clusters, while the C distribution is homogeneous in the sample surface. Mo particles are quasi-spherical, with a diameter in the order of hundreds of nanometers. SEM images are analyzed to extract the diameter of the particle as a function of the laser fluence and number of laser pulses in a sample in which 100 nm of Mo was initially deposited by sputtering. Results are presented in Figure 3e. Two samples with distinguished irradiation conditions are analyzed. The first sample was irradiated with 100 pulses of 0.189 J cm^{-2} (denominated as a high dosage), and the second sample was irradiated with 20 pulses of 0.122 J cm^{-2} (denominated as a low dosage). The size distribution histogram shows that, in the sample that was irradiated with 100 pulses of high fluence, formed Mo particles have a diameter between 350 and 550 nm. In the sample that was irradiated with 20 pulses of low fluence, formed Mo particles have a wider diameter distribution, which takes values between 100 and 500 nm. Observation of the SEM images of the above samples (Figure 3f) reveals that, in the sample irradiated with 100 pulses of high fluence, Mo particles are distributed with a lower density on the VGNWs and show a narrower size distribution (left panel of Figure 3f). In the sample irradiated with 20 pulses of low fluence, Mo particles are distributed with a higher density on the VGNWs. Moreover, in addition to these larger clusters, smaller particles are distributed on the basal plane of the VGNWs, which results in a wider size distribution (right panel of Figure 3f). A schematic representation presented in Figure 3g illustrates the morphology of each sample. For the sample irradiated with 100 pulses of high fluence, Mo receives enough energy to form distinguished large clusters via dewetting and subsequent merging of the Mo film (left panel of Figure 3g). For the sample irradiated with 20 pulses of low fluence, the same process occurs but without completing the merging and cluster formation. As a result, smaller particles remain on the basal planes of the graphene flakes, while the clustered particles formed on the edges of the VGNWs possess lower diameters on average (right panel of Figure 3g). In addition, high fluence pulses result in the detachment of materials as a result of thermal evaporation. EDS characterization is used to evaluate the Mo weight percentage of the above samples upon irradiation. Results are depicted in panels h and i of Figure 3. The Mo content is decreasing with the increase in both the number of pulses and pulse fluence. This is the case for films with thicknesses of both 50 and 100 nm.[33] The 100 nm thick film has an initial Mo weight percentage of 14.45%, which is reduced to 3.77% upon irradiation with the maximum number of pulses (100) of the highest fluence (0.186 J cm^{-2}) (Figure 3h). In a similar trend, the 50 nm thick film has an initial Mo weight percentage of 5.18%, which is reduced to 2.57% upon irradiation with the maximum number of pulses (100) of the highest fluence (0.186 J cm^{-2}) (Figure 3i). Lower weight percentage reduction rates are recorded when pulses of lower fluences (0.149 and 0.122 J cm^{-2}) are applied. These results demonstrate the capacity to control the mass of Mo particles on VGNWs via controlled pulsed laser irradiation.

Finally, structural modifications between the pristine and irradiated samples have been detected by X-ray diffraction (XRD) characterization, depicted in Figure 4. The Mo film

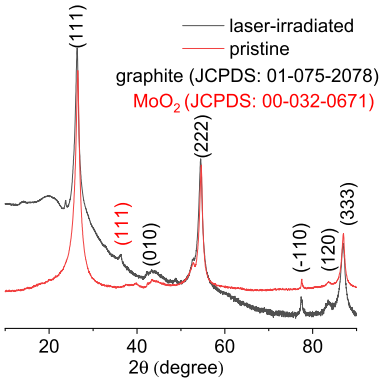

Figure 4. XRD characterization of pristine Mo deposited on VGNWs (red graph) and upon laser irradiation (black graph), revealing the formation of MoO_2 nanoparticles (NPs).

deposited by magneton sputtering is initially amorphous. Thus, the pristine sample of a 100 nm Mo film on VGNWs shows only diffraction peaks originating from the VGNWs and no diffraction peaks related to Mo compounds (red graph). Upon laser irradiation, the (111) diffraction peak of monoclinic MoO_2 appears at 36.35° [black graph, Joint Committee on Powder Diffraction Standards (JCPDS) file number 00-032-0671],[34,35] showcasing the partial crystallization of the resulting particles formed on the VGNWs. We argue that the formation of the Mo oxide phase occurs as a result of migration and reaction with oxygen species that are loosely bonded or physisorbed on defective sites of the VGNWs, as confirmed by X-ray photoemission spectroscopy in previous studies.[23] Surface heating as a result of laser irradiation induces migration and metal oxidation. EDS characterization reveals the presence of C, O, and Mo on the resulting irradiated nanostructures (Supplementary Figure 2 of the Supporting Information).

In conclusion, our research proposes a novel approach for the rapid functionalization of VGNWs through pulsed laser irradiation. The study systematically examines the impact of two critical irradiation parameters, namely, the number of applied pulses and the fluence of each pulse, on the physicochemical properties of VGNWs. Raman spectroscopy serves to characterize the changes in the chemical structure of VGNWs induced by irradiation. We observe that an increase in the number of pulses and fluence leads to a notable reduction in the density of defects and $fwhm_{2D}$. This phenomenon suggests a mechanism involving the evaporation of amorphous or loosely bonded carbon from defective points and subsequent recrystallization of the graphene lattice. Furthermore, our investigation extends to the effect of laser irradiation on Mo thin films deposited on the VGNWs. The received thermal dosage induces dewetting, evaporation, and clustering of Mo, resulting in the formation of particles with diameters of hundreds of nanometers according to SEM and EDS characterization. Importantly, we find that both the number of pulses and the pulse fluence significantly influence the size and distribution of these formed particles. This comprehensive study not only sheds light on the intricate mechanisms

https://doi.org/10.1021/acs.jpclett.4c00193
J. Phys. Chem. Lett. 2024, 15, 3779−3784

underlying the laser-induced modifications of VGNWs but also introduces a promising method for the rapid functionalization of VGNWs. The applicability of this approach extends beyond VGNWs and holds the potential for the functionalization of other graphene derivatives and carbon-based nanostructures. The findings presented here contribute to the evolving field of advanced materials and pave the way for further exploration of laser-based techniques in tailoring the properties of nanomaterials.[36,37]

■ ASSOCIATED CONTENT

Supporting Information

The Supporting Information is available free of charge at https://pubs.acs.org/doi/10.1021/acs.jpclett.4c00193.

Description of the experimental part, including detailed description on the synthesis of VGNWs, the laser irradiation setup and performed experiments, and the performed structural and morphological characterization, and two supplementary figures, including a SEM image of pristine VGNWs and an EDS spectrum of the Mo nanoparticles formed on the VGNWs (PDF)

Transparent Peer Review report available (PDF)

■ AUTHOR INFORMATION

Corresponding Author

Stefanos Chaitoglou − *Department of Applied Physics and ENPHOCAMAT Group, Institute of Nanoscience and Nanotechnology (IN2UB), University of Barcelona, 08028 Barcelona, Catalonia, Spain;* orcid.org/0000-0001-6074-1853; Email: stefanoschaitoglou@ub.edu

Authors

Argyro Klini − *Institute of Electronic Structure and Laser, Foundation for Research and Technology—Hellas, 70013 Heraklion, Greece*

Nikandra Papakosta − *Institute of Electronic Structure and Laser, Foundation for Research and Technology—Hellas, 70013 Heraklion, Greece*

Yang Ma − *Department of Applied Physics and ENPHOCAMAT Group, Institute of Nanoscience and Nanotechnology (IN2UB), University of Barcelona, 08028 Barcelona, Catalonia, Spain*

Roger Amade − *Department of Applied Physics and ENPHOCAMAT Group, Institute of Nanoscience and Nanotechnology (IN2UB), University of Barcelona, 08028 Barcelona, Catalonia, Spain*

Panagiotis Loukakos − *Institute of Electronic Structure and Laser, Foundation for Research and Technology—Hellas, 70013 Heraklion, Greece*

Enric Bertran-Serra − *Department of Applied Physics and ENPHOCAMAT Group, Institute of Nanoscience and Nanotechnology (IN2UB), University of Barcelona, 08028 Barcelona, Catalonia, Spain;* orcid.org/0000-0002-9694-3729

Complete contact information is available at: https://pubs.acs.org/10.1021/acs.jpclett.4c00193

Notes

The authors declare no competing financial interest.

■ ACKNOWLEDGMENTS

This project has received funding from the European Union's Horizon 2020 Research and Innovation Programme under Grant Agreement 871124 Laserlab-Europe. The ENPHOCAMAT group acknowledges financial support from Grant TED2021-132070B-C21, funded by the Spanish Ministry for Science and Innovation, and Grant 2021SGR00936, funded by the AGAUR of Generalitat de Catalunya. Yang Ma acknowledges the support from the Predoctoral Fellowship Program funded by the China Scholarship Council affiliated with the Ministry of Education of the People's Republic of China. Stefanos Chaitoglou acknowledges support from the Postdoctoral Fellowship Programme de Pinós, funded by the Secretary of Universities and Research (Government of Catalonia) through Grant Agreement 801370 (H2020-MSCA-COFUND-2017) and from the MSCA Fellowship funded by the European Commission through Grant Agreement 101062014 (HORIZON Europe-MSCA-2021-PF-01).

■ REFERENCES

(1) Urade, A. R.; Lahiri, I.; Suresh, K. S. Graphene Properties, Synthesis and Applications: A Review. *JOM* **2023**, *75*, 614−630.

(2) Aïssa, B.; Memon, N. K.; Ali, A.; Khraisheh, M. K. Recent Progress in the Growth and Applications of Graphene as a Smart Material: A Review. *Front. Mater.* **2015**, *2*, 58.

(3) Chen, W.; Lv, G.; Hu, W.; Li, D.; Chen, S.; Dai, Z. Synthesis and Applications of Graphene Quantum Dots: A Review. *Nanotechnol Rev.* **2018**, *7*, 157−185.

(4) Olabi, A.; Abdelkareem, M. A.; Wilberforce, T.; Sayed, E. T. Application of Graphene in Energy Storage Device—A Review. *Renewable Sustainable Energy Rev.* **2021**, *135*, 110026.

(5) Park, N.; Lee, H.; Park, J.; Chau, T. K.; Kang, H.; Kang, H.; Suh, D. Charge Carrier Modulation in Graphene on Ferroelectric Single-Crystal Substrates. *NPG Asia Mater.* **2022**, *14*, 58.

(6) Qin, Y.; Zhang, Z. Co-Modulation of Graphene by N Hetero-Doping and Vacancy Defects and the Effect on NO_2 Adsorption and Sensing: First-Principles Study. *Phys. E* **2020**, *116*, 113737.

(7) Chaitoglou, S.; Bertran, E. Effect of Temperature on Graphene Grown by Chemical Vapor Deposition. *J. Mater. Sci.* **2017**, *52*, 8348−8356.

(8) Guo, Y.; Zhang, C.; Chen, Y.; Nie, Z. Research Progress on the Preparation and Applications of Laser-Induced Graphene Technology. *Nanomaterials* **2022**, *12*, 2336.

(9) Wan, Z.; Streed, E. W.; Lobino, M.; Wang, S.; Sang, R. T.; Cole, I. S.; Thiel, D. V.; Li, Q. Laser-Reduced Graphene: Synthesis, Properties, and Applications. *Adv. Mater. Technol.* **2018**, *3*, 1700315.

(10) Vasquez, A.; Samolis, P.; Zeng, J.; Sander, M. Y. Micro-Structuring, Ablation, and Defect Generation in Graphene with Femtosecond Pulses. *OSA Continuum* **2019**, *2*, 2925−2934.

(11) Khandelwal, M.; Van Tran, C.; Lee, J.; In, J. B. Nitrogen and Boron Co-doped Densified Laser-Induced Graphene for Supercapacitor Applications. *Chem. Eng. J.* **2022**, *428*, 131119.

(12) Lin, J.; Peng, Z.; Liu, Y.; Ruiz-Zepeda, F.; Ye, R.; Samuel, E. L. G.; Yacaman, M. J.; Yakobson, B. I.; Tour, J. M. Laser-Induced Porous Graphene Films from Commercial Polymers. *Nat. Commun.* **2014**, *5*, 5714.

(13) Chaudhury, S.; Thakur, A. K.; Gojman, R. S.; Arnusch, C. J.; Nir, O. Ion Transport in Laser-Induced Graphene Cation-Exchange Membrane Hybrids. *J. Phys. Chem. Lett.* **2020**, *11*, 1397−1403.

(14) Pierpaoli, M.; Ficek, M.; Jakóbczyk, P.; Karczewski, J.; Bogdanowicz, R. Self-Assembly of Vertically Orientated Graphene Nanostructures: Multivariate Characterisation by Minkowski Functionals and Fractal Geometry. *Acta Mater.* **2021**, *214*, 116989.

(15) Kumar, R.; Pérez del Pino, A.; Sahoo, S.; Singh, R. K.; Tan, W. K.; Kar, K. K.; Matsuda, A.; Joanni, E. Laser Processing of Graphene and Related Materials for Energy Storage: State of the Art and Future prospects. *Prog. Energy Combust. Sci.* **2022**, *91*, 100981.

(16) Evlashin, S. A.; Fedorov, F. S.; Dyakonov, P. V.; Maksimov, Yu. M.; Pilevsky, A. A.; Maslakov, K. I.; Kuzminova, Yu. O.; Mankelevich, Yu. A.; Voronina, E. N.; Dagesyan, S. A.; Pletneva, V. A.; Pavlov, A. A.; Tarkhov, M. A.; Trofimov, I. V.; Zhdanov, V. L.; Suetin, N. V.; Akhatov, I. S. Role of Nitrogen and Oxygen in Capacitance Formation of Carbon Nanowalls. *J. Phys. Chem. Lett.* **2020**, *11*, 4859−4865.
(17) Cui, S.; Guo, X.; Ren, R.; Zhou, G.; Chen, J. Decoration of Vertical Graphene with Aerosol Nanoparticles for Gas Sensing. *J. Phys. D. Appl. Phys.* **2015**, *48*, 314008.
(18) Li, M.; Liu, D.; Wei, D.; Song, X.; Wei, D.; Wee, A. T. S. Controllable Synthesis of Graphene by Plasma-Enhanced Chemical Vapor Deposition and Its Related Applications. *Adv. Sci.* **2016**, *3*, 1600003.
(19) Chaitoglou, S.; Amade, R.; Ospina, R.; Bertran-Serra, E. Hybrid Nanostructured Compounds of Mo_2C on Vertical Graphene Nanoflakes for a Highly Efficient Hydrogen Evolution Reaction. *ACS Appl. Energy Mater.* **2023**, *6*, 6120−6131.
(20) Farid, G.; Amade, R.; Chaitoglou, S.; Alshaikh, I.; Ospina, R.; Ma, Y.; Bertran-Serra, E. Efficient Flexible Electrodes for Lithium-Ion Batteries Utilizing Well-Dispersed Hybrid Mo_2C Nanoparticles on Vertically-Oriented Graphene Nanowalls. *J. Alloys Compd.* **2023**, *968*, 172109.
(21) Chaitoglou, S.; Ospina, R.; Ma, Y.; Amade, R.; Vendrell, X.; Rodriguez-Pereira, J.; Bertran-Serra, E. Deposition and In-Situ Formation of Nanostructured Mo_2C Nanoparticles on Graphene Nanowalls Support for Efficient Electrocatalytic Hydrogen Evolution. *J. Alloys Compd.* **2024**, *972*, 172891.
(22) Amade, R.; Muyshegyan-Avetisyan, A.; González, J. M.; Pérez del Pino, A.; György, E.; Pascual, E.; Andújar, J. L.; Bertran Serra, E. Super-Capacitive Performance of Manganese Dioxide/Graphene Nano-Walls Electrodes Deposited on Stainless Steel Current Collector. *Materials* **2019**, *12*, 483.
(23) Chaitoglou, S.; Amade, R.; Bertran, E. Insights into the Inherent Properties of Vertical Graphene Flakes towards Hydrogen Evolution Reaction. *Appl. Surf. Sci.* **2022**, *592*, 153327.
(24) Chaitoglou, S.; Bertran, E. Effect of Pressure and Hydrogen Flow in Nucleation Density and Morphology of Graphene Bidimensional Crystals. *Mater. Res. Express* **2016**, *3*, No. 075603.
(25) Suemori, K.; Watanabe, Y.; Fukuda, N.; Uemura, S. Voltage Contrast in Scanning Electron Microscopy to Distinguish Conducting Ag Nanowire Networks from Nonconducting Ag Nanowire Networks. *ACS Omega* **2020**, *5*, 12692−12697.
(26) Mohiuddin, T. M. G.; Lombardo, A.; Nair, R. R.; Bonetti, A.; Savini, G.; Jalil, R.; Bonini, N.; Basko, D. M.; Galiotis, C.; Marzari, N.; Novoselov, K. S.; Geim, A. K.; Ferrari, A. C. Uniaxial Strain in Graphene by Raman Spectroscopy: G Peak Splitting Grüneisen Parameters and sample orientation. *Phys. Rev. B* **2009**, *79*, 205433.
(27) Cançado, L. G.; Jorio, A.; Ferreira, E. H. M.; Stavale, F.; Achete, C. A.; Capaz, R. B.; Moutinho, M. V. O.; Lombardo, A.; Kulmala, T. S.; Ferrari, A. C. Quantifying Defects in Graphene via Raman Spectroscopy at Different Excitation Energies. *Nano Lett.* **2011**, *11*, 3190−3196.
(28) Chaitoglou, S.; Bertran, E. Control of the Strain in Chemical Vapor Deposition-Grown Graphene over Copper via H_2 Flow. *J. Phys. Chem. C* **2016**, *120*, 25572−25577.
(29) Zhang, A.; Chen, T.; Song, S.; Yang, W.; Gooding, J. J.; Liu, J. Ultrafast Generation of Highly Crystalline Graphene Quantum Dots from Graphite Paper via Laser Writing. *J. Colloid Interface Sci.* **2021**, *594*, 460−465.
(30) Bertran-Serra, E.; Musheghyan-Avetisyan, A.; Chaitoglou, S.; Amade Rovira, R.; Alshaikh, I.; Pantoja-Suarez, F.; Andújar-Bella, J.-L.; Jawhari, T.; Perez-del-Pino, A.; Gyorgy, E. Temperature-Modulated Synthesis of Vertically Oriented Atomic Bilayer Graphene Nanowalls Grown on Stainless Steel by Inductively Coupled Plasma Chemical Vapour Deposition. *Appl. Surf. Sci.* **2023**, *610*, 155530.
(31) Bertran-Serra, E.; Rodriguez-Miguel, S.; Li, Z.; Ma, Y.; Farid, G.; Chaitoglou, S.; Amade, R.; Ospina, R.; Andújar, J.-L. Advancements in Plasma-Enhanced Chemical Vapor Deposition for Producing Vertical Graphene Nanowalls. *Nanomaterials* **2023**, *13*, 2533.
(32) Wang, L.; Chi, X.; Wang, X.; Liu, Q.; Sun, L. Preparing Ripening-Suppressed Metallic Nanoparticles Using a Laser Irradiated Carbon Nanotube Sacrificial Layer. *Appl. Surf. Sci.* **2020**, *506*, 144705.
(33) Stafast, H.; Von Przychowski, M. Evaporation of Solids by Pulsed Laser Irradiation. *Appl. Surf. Sci.* **1989**, *36*, 150−156.
(34) Moulahi, A.; Ibrahim, M. A.; Mjejri, I.; Al-Marri, A. H.; Sediri, F. Controlled Hydrothermal Synthesis of Nano-MoO_2 as Anode for Lithium-Ion Battery. *Indian J. Sci. Technol.* **2020**, *13*, 277−285.
(35) Li, Z. Q.; Lu, C. J.; Xia, Z. P.; Zhou, Y.; Luo, Z. X-ray Diffraction Patterns of Graphite and Turbostratic Carbon. *Carbon* **2007**, *45*, 1686−1695.
(36) Poimenidis, I. A.; Tsanakas, M. D.; Papakosta, N.; Klini, A.; Farsari, M.; Moustaizis, S. D.; Loukakos, P. A. Enhanced Hydrogen Production through Alkaline Electrolysis Using Laser-Nanostructured Nickel Electrodes. *Int. J. Hydrogen Energy* **2021**, *46*, 37162−37173.
(37) Poimenidis, I. A.; Papakosta, N.; Manousaki, A.; Klini, A.; Farsari, M.; Moustaizis, S. D.; Loukakos, P. A. Electrodeposited Laser—Nanostructured Electrodes for Increased Hydrogen Production. *Int. J. Hydrogen Energy* **2022**, *47*, 9527−9536.

https://doi.org/10.1021/acs.jpclett.4c00193
J. Phys. Chem. Lett. 2024, 15, 3779−3784